The Allosteric Regulation of pyruvate kinase by fructose-1,6-bisphosphate

ARTICLE *in* STRUCTURE · MARCH 1998

Impact Factor: 5.62 · DOI: 10.1016/S0969-2126(98)00021-5 · Source: PubMed

6 AUTHORS, INCLUDING:

Melissa S Jurica
University of California, Santa Cruz
53 PUBLICATIONS **2,436** CITATIONS
SEE PROFILE

Patrick J. Heath
Fred Hutchinson Cancer Research Center
13 PUBLICATIONS **604** CITATIONS
SEE PROFILE

Thomas Nowak
University of Notre Dame
69 PUBLICATIONS **1,707** CITATIONS
SEE PROFILE

The allosteric regulation of pyruvate kinase by fructose-1,6-bisphosphate

Melissa S Jurica[1], Andrew Mesecar[2], Patrick J Heath[3], Wuxian Shi[4], Thomas Nowak[5] and Barry L Stoddard[3]*

Background: Yeast pyruvate kinase (PK) catalyzes the final step in glycolysis. The enzyme therefore represents an important control point and is allosterically activated by fructose-1,6-bisphosphate (FBP). In mammals the enzyme is found as four different isozymes with different regulatory properties: two of these isozymes are produced by alternate splicing. The allosteric regulation of PK is directly related to proliferation of certain cell types, as demonstrated by the expression of an allosterically regulated isozyme in tumor cells. A model for the allosteric transition from the inactive (T) state to the active (R) state has been proposed previously, but until now the FBP-binding site had not been identified.

Results: We report here the structures of PK from yeast complexed with a substrate analog and catalytic metal ions in the presence and absence of bound FBP. The allosteric site is located 40 Å from the active site and is entirely located in the enzyme regulatory (C) domain. A phosphate-binding site for the allosteric activator is created by residues encoded by a region of the gene corresponding to the alternately spliced exon of mammalian isozymes. FBP activation appears to induce several conformational changes among active-site sidechains through a mechanism that is most likely to involve significant domain motions, as previously hypothesized.

Conclusions: The structure and location of the allosteric activator site agrees with the pattern of alternate genetic splicing of the PK gene in multicellular eukaryotes that distinguishes between a non-regulated isozyme and the regulated fetal isozymes. The conformational differences observed between the active sites of inactive and fully active PK enzymes is in agreement with the recently determined thermodynamic mechanism of allosteric activation through a 'metal relay' that increases the affinity of the enzyme for its natural phosphoenolpyruvate substrate.

Addresses: [1]Molecular and Cellular Biology Program of the University of Washington and Fred Hutchinson Cancer Research Center A3-023, 1124 Columbia Street, Seattle, WA 98104, USA, [2]Department of Molecular and Cell Biology, Stanley Hall, University of California, Berkeley CA 94720, USA, [3]Program in Structural Biology, Division of Basic Sciences, Fred Hutchinson Cancer Research Center A3-023, 1124 Columbia Street, Seattle, WA 98104, USA, [4]Department of Biochemistry and Molecular Biology, Pennsylvania State University, 152 Davey Lab, University Park, PA 16802, USA and [5]Department of Chemistry and Biochemistry, University of Notre Dame, Notre Dame, IN 46556, USA.

*Corresponding author.
E-mail: bstoddar@fhcrc.org

Key words: allostery, alternative splicing, isozyme shift, pyruvate kinase

Received: **15 October 1997**
Revisions requested: **24 November 1997**
Revisions received: **22 December 1997**
Accepted: **6 January 1998**

Structure 15 February 1998, **6**:195–210
http://biomednet.com/elecref/0969212600600195

Introduction

Pyruvate kinase (PK) catalyzes the final step in glycolysis, producing the second of two ATP molecules generated in the glycolytic pathway. The enzyme converts phosphoenolpyruvate (PEP) and ADP to pyruvate and ATP (Figure 1). This reaction is a committed step leading to either anaerobic fermentation or oxidative phosphorylation of pyruvate. In most cells the reaction is essentially irreversible ($K_{eq} = 10^3$ to 10^4) and is one of the major control points of glycolysis. The regulation of PK is important for controlling the levels of ATP, GTP and glycolytic intermediates in the cell. Pk also serves as a switch between the glycolytic and gluconeogenic pathways in certain tissues.

Allosteric regulation of enzyme activity is a mechanism for finely tuning biochemical reaction pathways in order to maintain an appropriate balance of intracellular substrate and product concentrations. Allosteric processes also allow an enzyme's activity to be coordinated with other cellular reactions and signaling pathways. As the metabolic requirements of an organism fluctuate over time and with cell type, many organisms produce related but differentially regulated forms of the same enzyme in different tissues to satisfy disparate metabolic and growth patterns.

PK is an example of such an enzyme: it can be isolated from mammalian tissues as four isozymes (L, R, M_1 and M_2). Each isozyme exhibits different kinetic properties that reflect the particular metabolic requirements of the expressing tissue. In humans, two genes (the L and M loci) encode the four different PK isozymes (Figure 2). The L gene encodes both the L isozyme found in liver and the R isozyme found in red blood cells, by use of a differential promoter [1]. The M gene encodes the M_1 and M_2 isozymes by alternative splicing [2]. Type M_1 predominates in skeletal muscle and brain, while the M_2 isozyme is found primarily in the rapidly proliferating fetal tissues. The M_2 isozyme is progressively replaced

Figure 1

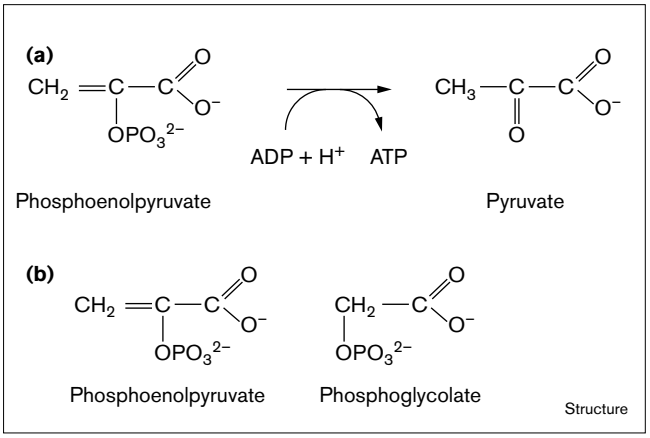

(a) The reaction catalyzed by PK. **(b)** The chemical structures of the substrate PEP and the substrate analog phosphoglycolate.

with the other tissue specific isozymes (M_1, R and L) during development. Type M_1 is regarded as non-regulated, because this isozyme shows predominantly non-sigmoidal Michaelis–Menten kinetic responses to the binding of all of its substrates and activators under most metabolic conditions. The M_2, L and R isozymes are regarded as allosterically regulated because of their sigmoidal kinetic responses to the binding of PEP, metal and fructose-1,6-bisphosphate (FBP). The M_2, R and L isozymes are allosterically regulated via feed-forward activation by FBP, the product of the phosphofructokinase (PFK) reaction. These forms are also allosterically regulated via feed-back inhibition by ATP, the product of the PK reaction, and by phosphorylation [3].

Allosteric regulation of PK is a critical feature of cell-cycle control in rapidly proliferating tissues, because PK controls both the consumption of metabolic carbon for biosynthesis and the utilization of pyruvate for energy production. Neoplasia of different tissues is associated with re-expression of the fetal M_2 isozyme [4]. Studies of human neuroectodermal (brain) tumors have revealed a shift from the M_1 isozyme, the dominant form in the adult human brain, to the M_2 isozyme [5,6]. This shift was found to be closely correlated with the histological grading, growth rate, and survival after resection of the tumor [7]. It has also been demonstrated that one characteristic marker of malignant human breast tumors is the re-expression of the allosterically regulated M_2 isozyme [8,9]. More recently, it was shown that the activity of PK in breast cancer cells is significantly increased compared to normal benign breast tissues [10].

Malignant cells have a high rate of aerobic glycolysis and biosynthesis. It has been suggested that the shift towards

Figure 2

PK isozymes and sequence alignment. **(a)** Expression of PK isoforms in humans. The type M_1 (non-regulated isozyme) and M_2 (allosterically regulated fetal and neoplastic isozyme) are produced from the same gene by differential splicing of the ninth and tenth exon into the final messenger RNA. **(b)** Sequence alignment of non-regulated muscle PK isozymes (1–3; orange) and allosterically regulated isozymes (4–6; black). Residues contacting FBP are marked by green arrows. Several of these residues are contributed by the alternatively spliced region in the human M_1 and M_2 isozyme sequence (blue box). The presence of a conserved glutamic acid residue (blue arrow) in the unregulated enzymes may act to prevent binding of the negatively charged FBP and/or mimic FBP binding. The secondary structure elements for the A and C domains are noted and labeled above the corresponding sequences.

the M_2 isozyme in tumors represents a mechanism to gain allosteric control of the enzyme and allows for sequential activation and inhibition of the enzyme during the cell cycle [11,12]. Inhibition may occur so that the cellular concentration of glycolytic intermediates may be elevated transiently, enhancing glucose breakdown via the hexose monophosphate shunt and accelerating synthesis of pyrimidine and purine nucleotides in proliferating cells.

The amino acid sequence of PK is highly conserved among all organisms (Figure 2). The human M_1 and M_2 protein sequences are encoded by an open reading frame composed of 12 exons and differ by only the alternate splicing of exons 9 and 10. These exon regions encode a stretch of 56 amino acids and comprise approximately one tenth of the total protein sequence (Figure 2). It is probable that this amino acid stretch forms the FBP-binding site and confers the different regulatory properties of the enzyme, as the M_1 form is non-regulated and does not bind FBP, whereas the M_2 is allosterically regulated by FBP. A putative FBP-binding site has been proposed based on indirect methods and observations but has yet to be structurally established [13–15]. Because the regulation of PK activity is a fundamental process in all cellular organisms and a classic example of the importance of allostery and tissue-specific isozyme variation, we have initiated an X-ray diffraction crystallographic study of various yeast PK (YPK) complexes. YPK shows an amino acid identity of 51% to the human M_2 isoform; it also exhibits the same pattern of allosteric regulation by FBP. This study describes the allosteric FBP-binding site and correlates the structural interactions at this site with measured ligand-binding energies and with patterns of differential expression of PK isozymes in mammalian tissues.

Results and discussion

Overall structural folds of YPK complexes

The structures of two YPK complexes were determined at 3.0 Å resolution as described in the Materials and methods. The first complex is a quaternary enzyme complex formed from YPK, Mn^{2+}, K^+ and the substrate

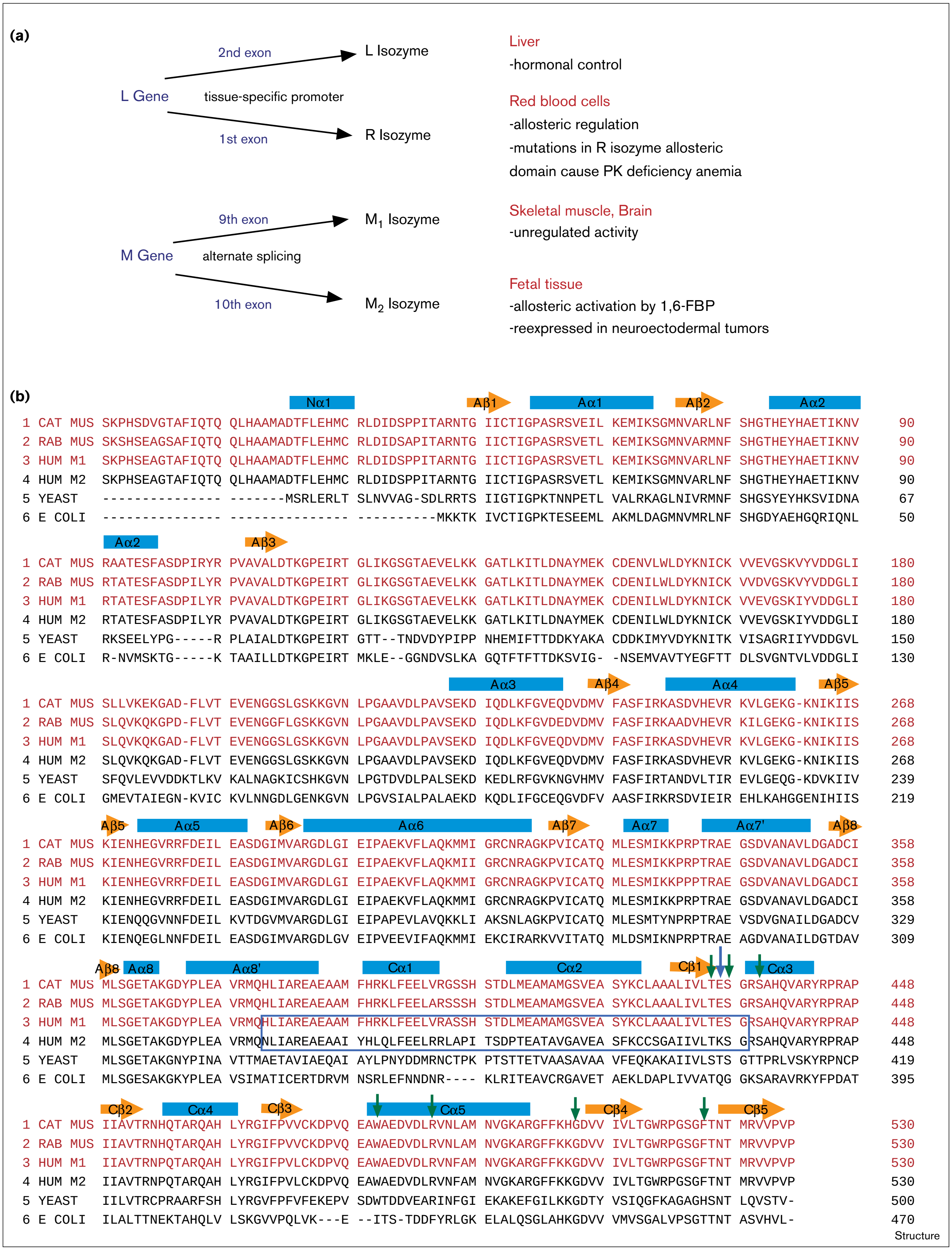
(a)
2nd exon
L Isozyme
L Gene
tissue-specific promoter
1st exon
R Isozyme
Liver
-hormonal control
Red blood cells
-allosteric regulation
-mutations in R isozyme allosteric
domain cause PK deficiency anemia
9th exon
M1 Isozyme
M Gene
alternate splicing
10th exon
M2 Isozyme
Skeletal muscle, Brain
-unregulated activity
Fetal tissue
-allosteric activation by 1,6-FBP
-reexpressed in neuroectodermal tumors
(b)
Nα1 Aβ1 Aα1 Aβ2 Aα2
1 CAT MUS SKPHSDVGTAFIQTQ QLHAAMADTFLEHMC RLDIDSPPITARNTG IICTIGPASRSVEIL KEMIKSGMNVARLNF SHGTHEYHAETIKNV 90
2 RAB MUS SKSHSEAGSAFIQTQ QLHAAMADTFLEHMC RLDIDSAPITARNTG IICTIGPASRSVETL KEMIKSGMNVARMNF SHGTHEYHAETIKNV 90
3 HUM M1 SKPHSEAGTAFIQTQ QLHAAMADTFLEHMC RLDIDSPPITARNTG IICTIGPASRSVETL KEMIKSGMNVARLNF SHGTHEYHAETIKNV 90
4 HUM M2 SKPHSEAGTAFIQTQ QLHAAMADTFLEHMC RLDIDSPPITARNTG IICTIGPASRSVETL KEMIKSGMNVARLNF SHGTHEYHAETIKNV 90
5 YEAST --------------- -------MSRLERLT SLNVVAG-SDLRRTS IIGTIGPKTNNPETL VALRKAGLNIVRMNF SHGSYEYHKSVIDNA 67
6 E COLI --------------- --------------- ----------MKKTK IVCTIGPKTESEEML AKMLDAGMNVMRLNF SHGDYAEHGQRIQNL 50
Aα2 Aβ3
1 CAT MUS RAATESFASDPIRYR PVAVALDTKGPEIRT GLIKGSGTAEVELKK GATLKITLDNAYMEK CDENVLWLDYKNICK VVEVGSKVYVDDGLI 180
2 RAB MUS RTATESFASDPILYR PVAVALDTKGPEIRT GLIKGSGTAEVELKK GATLKITLDNAYMEK CDENILWLDYKNICK VVDVGSKVYVDDGLI 180
3 HUM M1 RTATESFASDPILYR PVAVALDTKGPEIRT GLIKGSGTAEVELKK GATLKITLDNAYMEK CDENILWLDYKNICK VVEVGSKIYVDDGLI 180
4 HUM M2 RTATESFASDPILYR PVAVALDTKGPEIRT GLIKGSGTAEVELKK GATLKITLDNAYMEK CDENILWLDYKNICK VVEVGSKIYVDDGLI 180
5 YEAST RKSEELYPG-----R PLAIALDTKGPEIRT GTT--TNDVDYPIPP NHEMIFTTDDKYAKA CDDKIMYVDYKNITK VISAGRIIYVDDGVL 150
6 E COLI R-NVMSKTG-----K TAAILLDTKGPEIRT MKLE--GGNDVSLKA GQTFTFTTDKSVIG- -NSEMVAVTYEGFTT DLSVGNTVLVDDGLI 130
Aα3 Aβ4 Aα4 Aβ5
1 CAT MUS SLLVKEKGAD-FLVT EVENGGSLGSKKGVN LPGAAVDLPAVSEKD IQDLKFGVEQDVDMV FASFIRKASDVHEVR KVLGEKG-KNIKIIS 268
2 RAB MUS SLQVKQKGPD-FLVT EVENGGFLGSKKGVN LPGAAVDLPAVSEKD IQDLKFGVDEDVDMV FASFIRKAADVHEVR KILGEKG-KNIKIIS 268
3 HUM M1 SLQVKQKGAD-FLVT EVENGGSLGSKKGVN LPGAAVDLPAVSEKD IQDLKFGVEQDVDMV FASFIRKASDVHEVR KVLGEKG-KNIKIIS 268
4 HUM M2 SLQVKQKGAD-FLVT EVENGGSLGSKKGVN LPGAAVDLPAVSEKD IQDLKFGVEQDVDMV FASFIRKASDVHEVR KVLGEKG-KNIKIIS 268
5 YEAST SFQVLEVVDDKTLKV KALNAGKICSHKGVN LPGTDVDLPALSEKD KEDLRFGVKNGVHMV FASFIRTANDVLTIR EVLGEQG-KDVKIIV 239
6 E COLI GMEVTAIEGN-KVIC KVLNNGDLGENKGVN LPGVSIALPALAEKD KQDLIFGCEQGVDFV AASFIRKRSDVIEIR EHLKAHGGENIHIIS 219
Aβ5 Aα5 Aβ6 Aα6 Aβ7 Aα7 Aα7' Aβ8
1 CAT MUS KIENHEGVRRFDEIL EASDGIMVARGDLGI EIPAEKVFLAQKMMI GRCNRAGKPVICATQ MLESMIKKPRPTRAE GSDVANAVLDGADCI 358
2 RAB MUS KIENHEGVRRFDEIL EASDGIMVARGDLGI EIPAEKVFLAQKMII GRCNRAGKPVICATQ MLESMIKKPRPTRAE GSDVANAVLDGADCI 358
3 HUM M1 KIENHEGVRRFDEIL EASDGIMVARGDLGI EIPAEKVFLAQKMMI GRCNRAGKPVICATQ MLESMIKKPPPTRAE GSDVANAVLDGADCI 358
4 HUM M2 KIENHEGVRRFDEIL EASDGIMVARGDLGI EIPAEKVFLAQKMMI GRCNRAGKPVICATQ MLESMIKKPRPTRAE GSDVANAVLDGADCI 358
5 YEAST KIENQQGVNNFDEIL KVTDGVMVARGDLGI EIPAPEVLAVQKKLI AKSNLAGKPVICATQ MLESMTYNPRPTRAE VSDVGNAILDGADCV 329
6 E COLI KIENQEGLNNFDEIL EASDGIMVARGDLGV EIPVEEVIFAQKMMI EKCIRARKVVITATQ MLDSMIKNPRPTRAE AGDVANAILDGTDAV 309
Aβ8 Aα8 Aα8' Cα1 Cα2 Cβ1 Cα3
1 CAT MUS MLSGETAKGDYPLEA VRMQHLIAREAEAAM FHRKLFEELVRGSSH STDLMEAMAMGSVEA SYKCLAAALIVLTES GRSAHQVARYRPRAP 448
2 RAB MUS MLSGETAKGDYPLEA VRMQHLIAREAEAAM FHRKLFEELARSSSH STDLMEAMAMGSVEA SYKCLAAALIVLTES GRSAHQVARYRPRAP 448
3 HUM M1 MLSGETAKGDYPLEA VRMQHLIAREAEAAM FHRKLFEELVRASSH STDLMEAMAMGSVEA SYKCLAAALIVLTES GRSAHQVARYRPRAP 448
4 HUM M2 MLSGETAKGDYPLEA VRMQNLIAREAEAAI YHLQLFEELRRLAPI TSDPTEATAVGAVEA SFKCCSGAIIVLTKS GRSAHQVARYRPRAP 448
5 YEAST MLSGETAKGNYPINA VTTMAETAVIAEQAI AYLPNYDDMRNCTPK PTSTTETVAASAVAA VFEQKAKAIIVLSTS GTTPRLVSKYRPNCP 419
6 E COLI MLSGESAKGKYPLEA VSIMATICERTDRVM NSRLEFNNDNR---- KLRITEAVCRGAVET AEKLDAPLIVVATQG GKSARAVRKYFPDAT 395
Cβ2 Cα4 Cβ3 Cα5 Cβ4 Cβ5
1 CAT MUS IIAVTRNHQTARQAH LYRGIFPVVCKDPVQ EAWAEDVDLRVNLAM NVGKARGFFKHGDVV IVLTGWRPGSGFTNT MRVVPVP 530
2 RAB MUS IIAVTRNHQTARQAH LYRGIFPVVCKDPVQ EAWAEDVDLRVNLAM NVGKARGFFKKGDVV IVLTGWRPGSGFTNT MRVVPVP 530
3 HUM M1 IIAVTRNPQTARQAH LYRGIFPVLCKDPVQ EAWAEDVDLRVNFAM NVGKARGFFKKGDVV IVLTGWRPGSGFTNT MRVVPVP 530
4 HUM M2 IIAVTRNPQTARQAH LYRGIFPVLCKDPVQ EAWAEDVDLRVNFAM NVGKARGFFKKGDVV IVLTGWRPGSGFTNT MRVVPVP 530
5 YEAST IILVTRCPRAARFSH LYRGVFPFVFEKEPV SDWTDDVEARINFGI EKAKEFGILKKGDTY VSIQGFKAGAGHSNT LQVSTV- 500
6 E COLI ILALTTNEKTAHQLV LSKGVVPQLVK---E --ITS-TDDFYRLGK ELALQSGLAHKGDVV VMVSGALVPSGTTNT ASVHVL- 470

analog phosphoglycolate (PG). The second complex is a quinternary enzyme complex formed from YPK, Mn^{2+}, K^+, PG and the allosteric activator FBP. Both enzyme complexes were co-crystallized with substrates and activators to yield closely related monoclinic space groups with two monomers per asymmetric unit. The structures of both complexes are homotetramers and have overall conformations similar to the previously solved structures of the non-allosterically regulated muscle enzymes [16,17]. Each subunit of YPK is composed of four separate domains (Figure 3). The first domain, N, is a short α-helical stretch at the N terminus (residues 1–18) that is also present in the non-regulated muscle enzymes but is not present in the similarly FBP-activated enzyme from *Escherichia coli* [15]. The second domain, A, is the catalytic domain and is formed by two separate stretches of amino acids (residues 19–88 and 189–360) that fold together into the common parallel $(\alpha/\beta)_8$ barrel motif with two additional α helices. The third domain, B, is the capping domain (residues 89–188) and is a small nine-stranded β-barrel motif that forms a cap over the active site. Finally, the C domain, or the regulatory domain, is located at the C terminus of the protein (residues 361–500) and has an α/β open-sheet motif. In both YPK structures no ordered electron density is observable for the residues (11–16) connecting the N and A domains. In addition, in the quinternary complex, residues 160–161 of the B domain are not observable in either subunit, and residues 99–100 are not observable in one subunit. Conversely, in the quaternary complex without FBP, much of a long protein loop forming part of the allosteric binding site (residues 446–452) is disordered, as is the last loop of the C domain (485–493). Because these regions are visible in the presence of bound FBP and several residues from each loop contact the allosteric activator, this binding site appears to undergo a disorder→order transition during the allosteric activation of YPK (see below).

Allosteric effector FBP-binding site

A putative FBP-binding site for allosterically regulated PK has been proposed from a variety of indirect methods and from an analysis of the structures of the unliganded enzymes from cat muscle and *E. coli* [13–15]. The location of the FBP site was proposed to be in a cleft between the A and C domains. The crystal structure of the fully ligated, quinternary complex of YPK reveals that the FBP site actually lies completely within the C domain. One molecule of FBP was found in a binding pocket within the C domain of each monomer of the enzyme when co-crystallized with FBP. The density for each bound activator molecule was strong and unambiguous, as observed in unbiased F_o–F_c difference maps that were calculated after refinement of protein coordinates (Figure 4). FBP has been shown to display negative cooperativity in binding to YPK, with a stoichiometry of between three and four molecules bound per enzyme tetramer (Figure 5) [18]. In the crystal structure, any differential occupancy of FBP-bound sites is averaged over the four sites.

The electron density of the bound FBP supports modeling and refinement of the activator in the β-furanose form (Figure 4). This anomer was previously suggested as the activating stereoisomer of the compound on the basis of several biochemical studies [19–21].

The allosteric site for FBP is located ≅ 40 Å away from the active site within the same monomer. The FBP site is located in a pocket formed from a loop (residues 402–407) between the Cβ1 strand and the Cα3 helix, and from the first two turns of the Cα5 helix (Figure 3). This helix immediately follows a disordered loop (residues 446–452) that becomes ordered upon the binding of FBP (Figure 3). FBP binds in a pocket at this site and is almost completely buried. The 1′-phosphate group of FBP makes a strong 2.8 Å electrostatic interaction with Arg459. The 6′-phosphate makes a series of hydrogen bonds to the sidechains of Ser402, Ser404, and Thr407 (Figure 4). This sequence (Ser402-Thr-Ser-Gly-Thr-Thr407) thus constitutes a well defined phosphate-binding pocket in the enzyme. The sugar ring of the FBP molecule is deeply sequestered within the binding cavity, making a pair of hydrogen-bond contacts between hydroxyl oxygens and mainchain atoms of residues 483 and 491.

One additional interaction between the enzyme and FBP is formed by Trp452 and the furanose ring of FBP. Such an interaction would explain the large quenching and red shift in the Trp452 fluorescence spectrum that occur upon FBP binding [22], as well as the observed decrease in solvent accessibility of Trp452 [18].

Residues 446–452, including the tryptophan residue, are disordered in the absence of bound FBP. This sequence is positioned between the Cβ3 strand and the Cα5 helix and forms virtually no interactions with other protein residues allowing it to swing freely in solvent. This mobile loop is highly variable among organisms in both its length and its amino acid composition [18]. Sequence alignments indicate that the longest loops occur in enzymes isolated from fungi [18]; this loop is slightly shorter in the enzyme from higher eukaryotes, and shortest in the enzyme from protozoa and bacteria.

A comparison of the FBP-binding site of YPK with the same region in other PK structures reveals significant differences. In the quaternary structure of YPK determined in the absence of FBP, no electron density was observed for the residues in the above mobile loop at any stage of the structure determination and refinement. The turn of residues 487–493 is also disordered in the quaternary structure. The same site in the structure of the rabbit muscle

Figure 3

YPK structural model. **(a)** Stereo view of the tetrameric YPK with bound PG and bound FBP. The A domain is colored red, and the B and C domains are colored green and blue, respectively. Residues corresponding to the sequence encoded by the alternatively spliced exon in humans are colored purple; bound ligands are shown as gray van der Waals models. **(b)** Stereo view of a single YPK subunit showing the distance and relationship between the allosteric and active sites. PG, Mn^{2+} and K^{+} are bound in the active site between the A and B domains and FBP is bound in the allosteric site in the C domain. **(c)** Stereo view of the allosteric site with bound FBP. The arrow indicates the mobile loop that is disordered in the quaternary structure (i.e. without bound FBP).

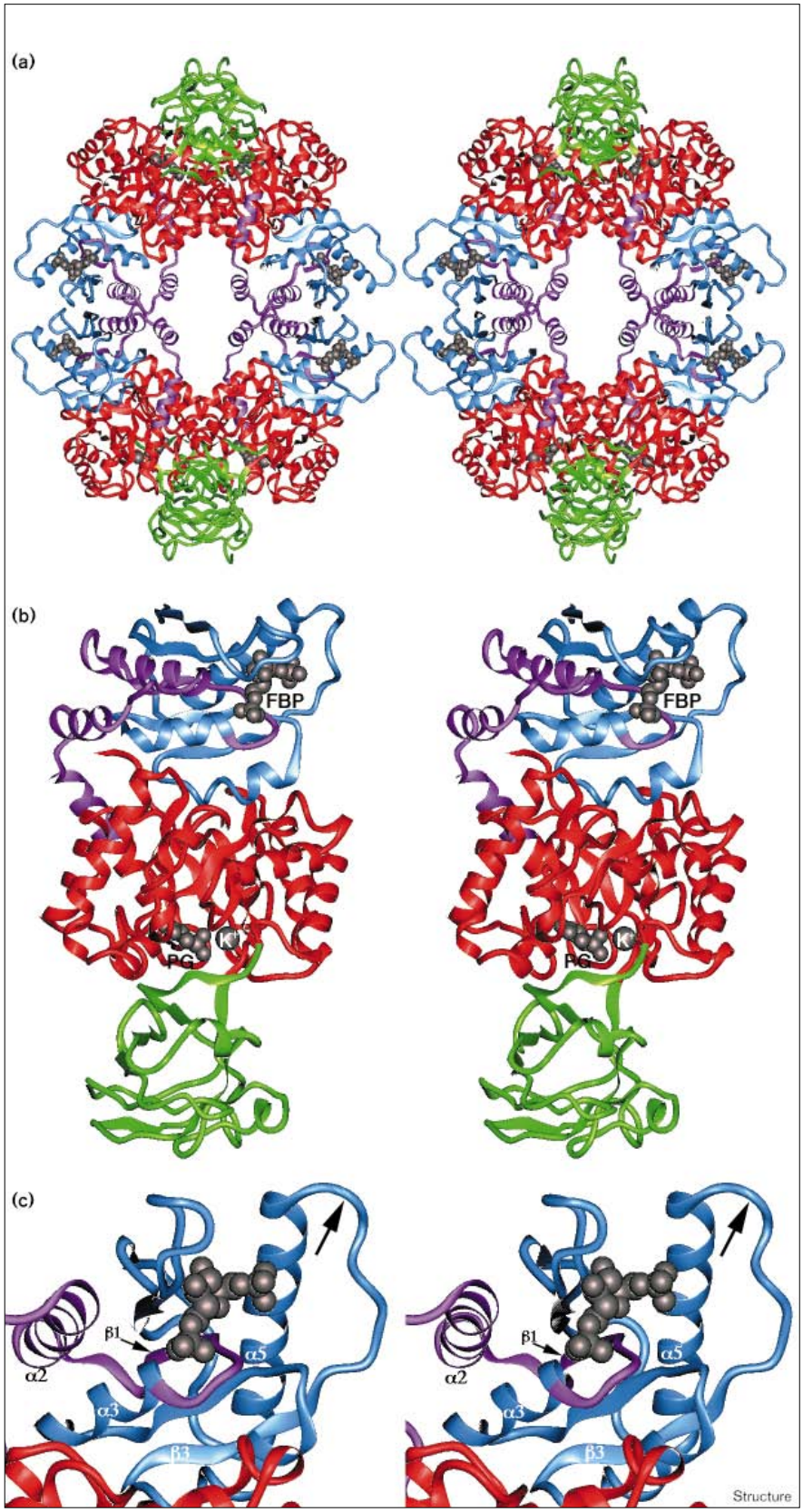

Figure 4

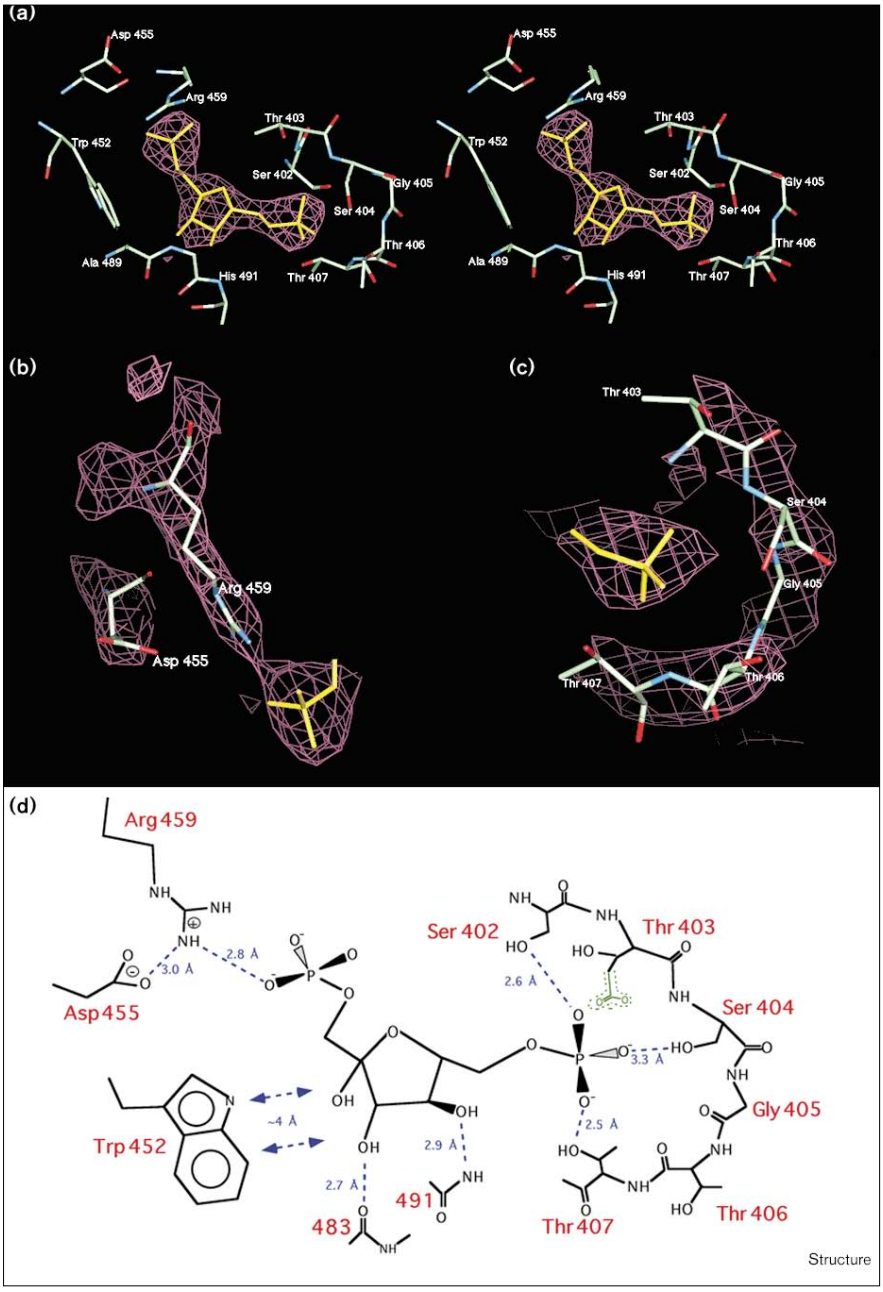

The FBP-binding site. **(a)** Stereo view of the allosteric activator binding site with bound FBP. Electron density ($2F_o–F_c$) is shown for FBP (yellow stick model) at a 1.5σ contour level. **(b)** Interaction of Arg459 and the FBP 1′-phosphate (shown in yellow). **(c)** Interaction of the FBP 6′-phosphate (yellow) with residues from the allosteric exon (403–407). **(d)** Schematic of the FBP-binding interactions. Interactions are shown as dashed blue lines and their distances are given in Å. Thr403 is converted to a glutamic acid in all known, sequenced non-allosteric isozymes. This residue is found in the alternatively spliced exon for the human M_2 isozyme. As a glutamic acid, this residue could either hinder FBP binding, through steric and electrostatic overlap, or act to mimic the effect of FBP binding.

enzyme, which is not regulated by FBP, shows a narrower pocket with the mobile loop shifted inwards. The turn of residues 487–493 in the rabbit structure is folded over the allosteric site thereby closing it off to FBP binding. The allosteric site in the *E. coli* apoenzyme structure differs primarily in that the mobile loop is truncated by six residues. Thus, there is no equivalent residue to Trp452 which contacts the sugar ring of FBP. Nevertheless, the phosphate-binding pocket (residues 402–407) for the 1′-phosphate of FBP is present in a similar conformation. Thr406, which is a lysine residue in the *E. coli* sequence, has previously been implicated in FBP binding by chemical modification and as a result of studies with the *E. coli* enzyme [14,23]. There is, however, no equivalent residue to Arg459 which binds the 6′-phosphate of FBP; in *E. coli* PK the Cα5 helix that donates this sidechain is shifted by over 2 Å away from the allosteric site.

The allosteric site for FBP is consistent with the location of the residues encoded by the alternatively-spliced exon

Figure 5

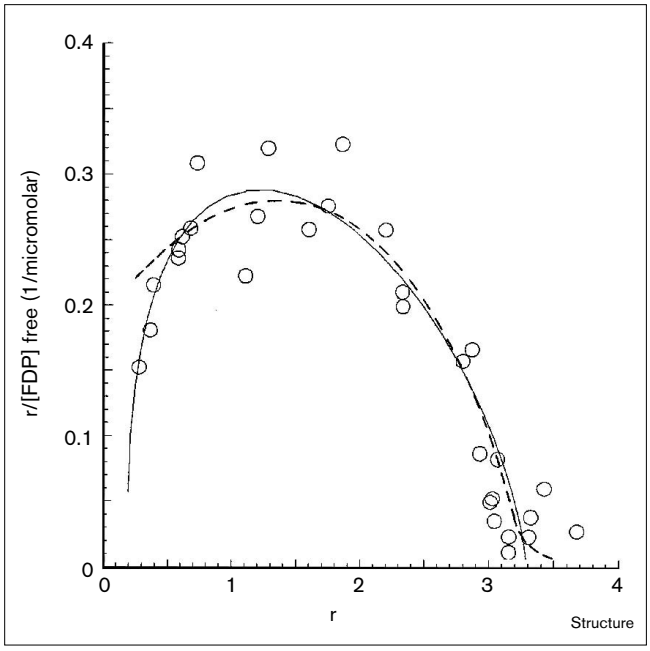

Binding effects of FBP. Scatchard binding plot for FBP in the presence of PEP and Mn^{2+}. The solid curve was generated by a best fit of the data to the Hill equation; the dotted curve represents the best fit of the data to the Adair equation, $r = [FBP]_{bound} / [YPK]_{total}$. Binding assays reproducibly indicate a combination of positive and negative cooperativity between binding sites, with a saturated stoichiometry of approximately three FBP molecules bound per tetramer under various conditions.

Figure 6

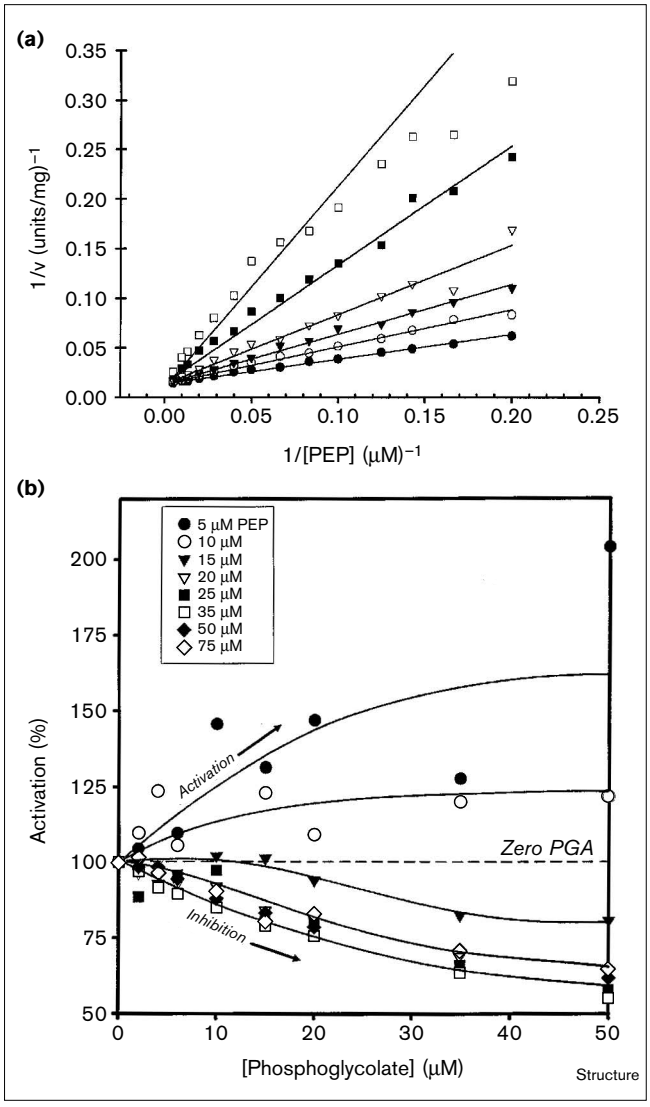

Inhibition and activation of YPK by PG. **(a)** Double reciprocal plot of the activity of YPK in the presence of 10 mM FBP measured by varying the concentration of PEP at different fixed concentrations of PG. PEP concentrations varied from 5 to 200 μM and PG concentrations were 0 (●), 10 (○), 20 (▼), 40 (▽), 100 (■), and 160 (□) μM, respectively. The data were best fit to a competitive inhibition model and the resulting kinetic constants are described in the text. **(b)** Plot of the relative percentage activation of YPK by PG in the absence of FBP. PEP concentrations were fixed between 5 and 75 μM (see insert) and PG concentrations were varied between 0 and 50 μM. The percentage activation was calculated by dividing the rates in the absence of PG by the rates in the presence of PG. At subsaturating PEP concentrations PG activates YPK and at high PEP concentrations PG inhibits YPK (see text for a detailed explanation). The lines are smooth curves through the data.

in mammalian PK isozymes. This stretch of amino acids, residues 349 to 405 in the yeast sequence, dictates the regulatory properties of the human muscle isozymes M_1 and M_2 (Figure 2). Within this region, residues 401 to 404 form one side of the binding cleft and a phosphate-binding pocket for the 1′-phosphate of FBP. These residues correspond to the last five amino acids encoded by the exon that is alternatively spliced. Ser402, which makes a hydrogen bond to the FBP 1′-phosphate, is conserved as a serine or threonine in mammalian M_2 PK sequences. Conversely, residue 403, which is a threonine in the yeast structure and a lysine in the human M_2 isozyme, is strictly conserved in non-regulated PK isozymes as a glutamic acid. This residue could hinder FBP binding through steric and electrostatic overlap and also could act in mimicking the effect of FBP binding.

The active site and binding of PG and catalytic metals

PG is a structural analog of PEP and has been shown to be a product of the YPK-catalyzed phosphorylation of glycolate by ATP [24] (Figure 1). In addition to being a substrate for the reverse reaction of YPK, PG is also a potent competitive inhibitor of PEP for the forward reaction (Figure 6a). The PG inhibition data is best fit to a model for linear competitive inhibition and the resulting steady-state kinetic parameters are $V_{max} = 72.3 \pm 0.7$ units/mg, $K_{M,PEP} = 19.3 \pm 0.6$ μM and $K_{I,PG} = 20.9 \pm 0.8$.

Figure 7

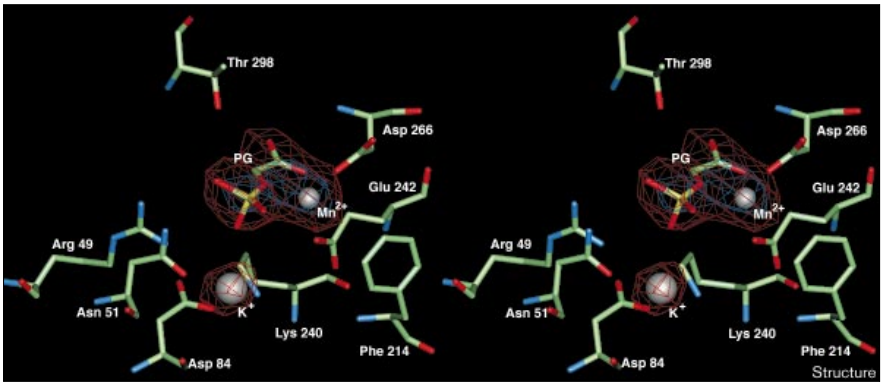

Stereo view of the active site of YPK with bound PG, Mn^{2+} and K^+. An electron-density ($2F_o–F_c$) map is shown at the 1.5σ contour level (red) and the 3.5σ contour level (blue). Atoms are shown in standard colors and metal ions are depicted as gray spheres.

The equivalence of K_M and K_I suggests that the binding modes of PEP and PG with YPK are very similar. In the absence of FBP and at subsaturating PEP concentrations, PG acts as an allosteric activator (Figure 6b). The KNF (Koshland–Nemethy–Filmer) or sequential model for the allosteric, homotropic activation of an enzyme by its substrate predicts that a substrate analog or competitive inhibitor may activate the enzyme in the absence of an allosteric activator under subsaturating substrate conditions [25]. The data in Figure 6 shows that at low, subsaturating PEP concentrations and at low PG concentrations, PG binds to YPK and increases the affinity of PEP for the remaining sites thereby increasing the activity. This is illustrated by the upward-curving portion of the data that rises above 100% activation. As PG concentrations are increased, it competes against PEP for the catalytic sites on the enzyme surface (shown by the downward-curving data). When PEP concentrations are saturating, PG competes for PEP at all of the active sites. The inhibition and activation data indicate that PG does indeed mimic the binding and allosteric activation of PEP.

Both of the crystallographically unique substrate-binding sites are occupied by bound PG, Mn^{2+}, and K^+ (Figure 7). The active site is located in a cleft between the A and B domains, as shown previously in both the cat and rabbit muscle enzymes [16,17,26]. Electron density associated with PG, Mn^{2+}, and K^+ appears in this same region of the map for YPK. PG was modeled into the density in a position analogous to that of pyruvate in the active site of rabbit muscle PK (complexed with Mn^{2+}, K^+ and pyruvate) [16]. The electron density for the phosphate group was very strong (>4σ). The position of the phosphate group is consistent with that of the 2-keto oxygen of pyruvate, which is formed after phosphoryl transfer from PEP to ADP. The orientation of PG and of its phosphate group also appears very similar to that of phospholactate in the recent rabbit M1 isozyme structure complexed in the presence of Mn^{2+}, and K^+ [26].

The electron density for the phosphate of PG places it in an electrostatic pocket formed by the positively charged sidechains of Arg49 and Lys269, and the monovalent and divalent metal ions, K^+ and Mn^{2+}, that are essential for enzymatic activity (Figure 7). Arg49 and Lys269 are 100% conserved in all PKs studied to date [18]. This positively charged electrostatic pocket would allow for the dissipation of the negative charges of the phosphate group during approach of the transition state, thereby making the phosphorous atom more electrophilic and susceptible to nucleophilic attack by ADP [27]. Thus, Arg49, Lys269, K^+, Mn^{2+}, and possibly Ser213, may serve to position and activate the phosphoryl transfer process.

Phosphoryl transfer has been shown to precede proton transfer and occurs via an 'in-line' associative pathway with inversion of configuration of the phosphorous center [28,29]. The products of the phosphoryl transfer process are proposed to be ATP and the enolate of pyruvate [30,31]. This intermediate is proposed by a number of studies to be protonated by either Lys240 or by Thr298 [16]. These residues are 100% conserved in all PKs and our structure supports the possibility that either residue may serve as a proton donor. A more definitive assignment of the proton donor will have to await further chemical, biophysical and site-directed mutagenesis studies.

There are some small differences in the orientation of the PG versus pyruvate in the rabbit M_1 structure (Figure 8). These differences are likely to be due to the negatively charged phosphate group of PG: its interaction with a positively charged binding pocket anchors it in a different orientation compared to the uncharged carbonyl oxygen at the analogous position in pyruvate. Moreover, PG lacks the methyl group of pyruvate which will also influence its relative orientation. As the carboxylate moiety is conserved between both PG and pyruvate, its position may be strongly dependent on the nature of the other atoms attached to the ligand.

Figure 8

Stereo view comparison of PK active sites. The figure shows a superposition of the PK active sites from yeast with bound PG, Mn^{2+} and K^+ (blue), rabbit muscle with bound pyruvate, Mn^{2+} and K^+ (red) and the *E. coli* apoenzyme (green).

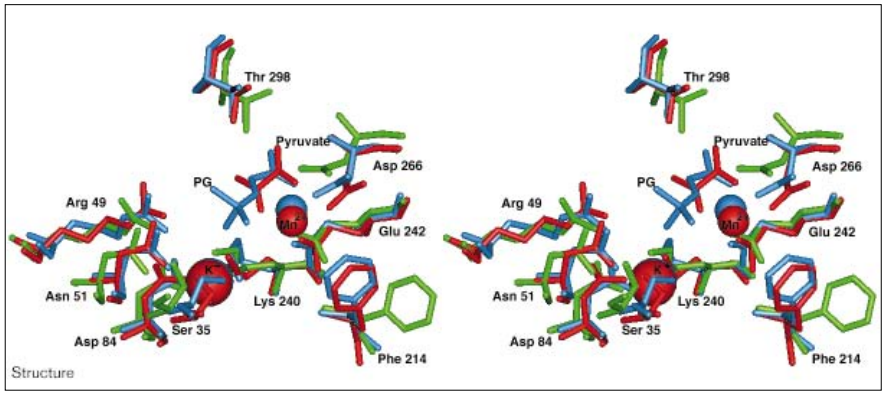

All known PKs have an absolute requirement for two divalent metal ions per monomer, usually Mg^{2+} or Mn^{2+}. In addition most PKs require one monovalent metal ion per monomer for activity, usually K^+ or NH_4^+ [32,33]. One of the divalent metal ions binds to the free enzyme and facilitates the binding of the substrate PEP while the other divalent metal binds to the enzyme via a complex with the substrate ADP [22,34–36]. YPK has an absolute requirement for both divalent and monovalent cations. The enzyme-bound divalent metal ion has been shown recently to trigger the allosteric activation of YPK through a metal ion mediated allosteric relay mechanism [22,36].

The enzyme-bound Mn^{2+} lies at the top of the α/β barrel in both the quaternary and quinternary structures of YPK. The coordination sphere of Mn^{2+} is approximately octahedral and is formed by two carboxylate sidechain oxygens of Glu242 (2.1 Å) and Asp266 (2.1 Å), one of the carboxylate oxygens of PG (2.0 Å), and the phosphoester oxygen of PG (2.1 Å). Two water molecules presumably complete the coordination but are not visible in the electron density at this resolution. The sidechain carboxylates of Glu242 and Asp266 chelate to the metal via their *anti* lone pairs [37]. The coordination sphere of Mn^{2+} observed in the yeast structures is similar to the coordination sphere of Mn^{2+} found in the rabbit muscle PK structures [16,26].

The Mn^{2+} site lies approximately 5.7 Å away from the K^+ site in both the quaternary and quinternary YPK structures. This is consistent with the range of distances between the enzyme-bound Mn^{2+} and Tl^+ sites of various YPK complexes calculated from NMR data [38]. The K^+ site is formed from residues located in two highly conserved stretches of amino acids. The first amino acid stretch, Asn51-Phe-Ser-His-Gly55, is 100% conserved in 28 PK sequences [18]. K^+ coordinates with the amide oxygen of Asn51 (2.9 Å) and with the sidechain oxygen of Ser53 (3.4 Å). The second amino acid stretch, Leu83-*Asp*-Thr-Lys-*Gly*-*Pro*-Glu-*Ile*-*Arg*-Thr92, is 100% conserved in 26 PK sequences and, considering only the italicised residues, 100% conserved in 28 PK sequences [18]. K^+ coordinates to a sidechain oxygen of Asp84 (2.8 Å) and to the backbone carbonyl oxygen of Thr85 (3.25 Å). Interestingly, the two PKs that differ in this stretch, enzymes isolated from *E. coli* (type II) and *Corynebacterium glutamicum*, are not activated by monovalent cations [39,40]. The sequence of this region in these two enzymes is Ala83-*Asp*-Leu-Gln-*Gly*-*Pro*-Lys-*Ile*-*Arg*-Val/Leu92. The substitution of lysine for glutamate at position 89 may activate the enzyme if the ε-NH_3^+ group of lysine takes the role of either K^+ or NH_4^+. We tested this possibility by modeling a lysine residue into the position of Glu89, where one of its carboxylate oxygens is 5.4 Å away from the K^+ site and 4.5 Å away from the phosphate site. Substituting a lysine residue for Glu89 places the ε-amino group within 2.4 Å of the existing K^+ site and in direct contact (3.0–3.3 Å) with one of the phosphate oxygens of the substrate. In addition, the ε-amino group position can be stabilized by forming a hydrogen bond (2.7 Å) with the absolutely conserved residue Ser53. Thus, a lysine residue in this position may indeed mimic the monovalent cation and assist in stabilizing phosphoryl transfer.

The nucleotide-bound Mn^{2+} site was not observed in electron density difference maps. This is consistent with the fact that Mn^{2+} binding to the second metal site is highly dependent on the presence of ADP [41,42]. Ligands that may serve to bind the nucleotide-bound metal and associated phosphates of ADP are Asn51 and His54, also part of the highly conserved loop between the Aβ2 strand and the Aα2 helix, and possibly Arg91, which is close to His54. These residues are close to the phosphate pocket of PG. Arg91 is 100% conserved in all PK sequences and it makes a hydrogen bond with the sidechain of Asp89 described above. Histidine residues have been proposed to be close to the nucleotide-bound metal site and to the adenine-binding site [43]. Furthermore, the nucleotide-bound Mn^{2+} site has been calculated from NMR studies to be

approximately 5–5.5 Å away from the enzyme-bound divalent cation site, approximately 5.9 Å away from the phosphate of PEP, and approximately 6.7 Å away from the monovalent cation site [44–46]. The conserved Asn51-Phe-Ser-His-Gly55 loop is located in a position consistent with these distances and may therefore participate in binding the Mn^{2+}AD(T)P complex.

It is difficult, however, to infer a precise location of the substrate AD(T)P from our structure or from the results of chemical modification studies. Three lysine residues of PK have been implicated in binding and/or catalysis of AD(T)P based on chemical modification studies of the enzyme with dialdehyde-AD(T)P. One homologous lysine residue that is subject to chemical modification is Lys337 [44–49]. This lysine is conserved in 22 out of 25 PK sequences and is in equivalent positions in all PK enzyme structures [18]. The residue is located near the entrance to the active site and resides in a loop between the two Aα8 helices, which is approximately 13 Å away from the phosphate of PG. The two additional lysine residues identified by chemical modification in the *E. coli* enzyme are Lys194 and Lys196 (*E. coli* sequence). Lys194 is present in all PK's, except the R and L forms encoded by the L gene in mammals, while Lys196 is present in only a few PK species. These two residues are over 20 Å away from Lys337. Without direct structural observation of ADP at the active site, it is difficult to ascertain how the substrate could occupy two completely different locations. What is notable, however, is that PK does not seem to show an absolute specificity towards any individual nucleotide diphosphate as ADP, GDP, UDP, IDP, TDP, and CDP can all serve as substrates [39,50–52]. This fact, together with NMR data on the conformation of enzyme-bound MgATP, suggest that the nucleotide portion of the NDP substrate may exhibit a high degree of mobility [53].

The structures of the active sites of YPK in the presence and absence of bound-FBP are extremely similar. The root mean square (rms) deviation between all atoms in these active sites is less than 1 Å. These results indicate that the structural effects of FBP binding are similar to the effects of cooperative substrate binding, in that either FBP or PEP can drive the enzyme towards a predominantly activated conformation. The simultaneous binding of Mn^{2+} and PEP to the YPK–K^+ complex is favored by –3.8 kcal/mol over the sum of their independent binding free energies. Similarly, the simultaneous binding of Mn^{2+}, PEP and FBP to the YPK–K^+ complex is favored by –6.6 kcal/mol [36]. The difference in coupling free energy of –2.8 kcal/mol between formation of the quaternary and quinternary complexes suggests that the small structural differences in the active-site complexes may be significant in terms of binding energies and affinities, although their steady-state catalytic rates are the same [22].

YPK exhibits little or no difference in the catalytic rates between the FBP-bound and unbound complexes under saturating substrate concentrations, in agreement with the structural comparison of the two complexes described above. However, this may be true only with its physiological substrate PEP. YPK-catalyzed phosphorylation of glycolate by ATP has been shown to occur only in the presence of FBP [24]. Differences in the microscopic rate constants for proton and phosphoryl transfer between PEP and ADP have been shown to be different for YPK in the presence and absence of FBP, even though the overall steady-state kinetic rates are the same [54]. PEP-bound YPK may undergo additional conformational changes at its active site upon the binding of FBP. We propose that these changes may fine-tune substrate alignment and hence the individual rate constants for both proton and phosphoryl transfer. The conformational changes and their effect on rate may be more dramatic with alternate substrates. Small conformational changes in protein structure and substrate orientation have been shown recently to have dramatic effects on the rate constants for enzyme-catalyzed reactions [55].

Allosteric activation of PK

YPK is regulated allosterically by a number of physiological effectors including PEP, ATP, H^+, Mn^{2+}, K^+ and FBP. Many of the interactions between these ligands and the enzyme involve both homotropic and heterotropic cooperativity [22,56,57]. YPK behaves as a classical 'K type' system, indicating that the substrates and allosteric activators modulate the binding affinities of each other. The allosteric activator FBP was originally thought to regulate YPK by 'directly' influencing the affinity of the enzyme for the substrate PEP. It was recently shown, however, that the major driving force for YPK regulation by FBP occurs through the enzyme-bound divalent metal via an allosteric relay mechanism [22,36].

A hypothesis regarding the mechanism of allosteric communication between the FBP- and PEP-binding sites has been previously proposed by comparing the structure of an inactivated (T state), PK structure from *E. coli* to the unregulated, active structures of PK from mammalian muscle tissues [15,58]. This model involves rotations of the catalytic and C-terminal domains of the enzyme by 17° and 15°, respectively, relative to the principle symmetry axes of the enzyme tetramer. It was proposed that highly conserved residues at the subunit interfaces (many of which are contributed by the alternatively spliced exon in mammals) couple conformational changes in the allosteric binding site to corresponding conformational changes in the active site, leading to an increase in the affinity for the PEP substrate. The recent structure of rabbit muscle PK complexed with phospholactate and metals in its active site also supports the concept of domain movements playing a functional role in the enzyme's activity [26]. It is

Figure 9

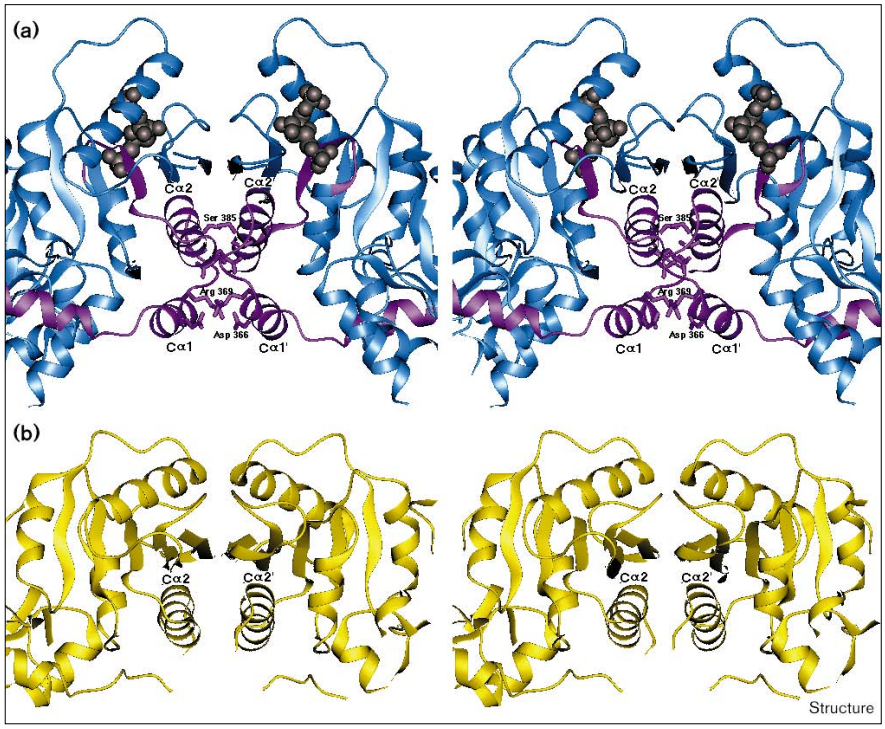

Stereo view of **(a)** one of the 'dimer-of-dimers' interfaces of the YPK activated tetramer (blue) and **(b)** the *E. coli* inactive tetramer (yellow). The human allosteric exon-encoded region is colored in purple on the yeast structure; bound ligands are shown as gray van der Waals models. The interacting sidechains from Cα1 and Cα2 are shown in the yeast structure. Sidechains from these helices in the *E. coli* structure are separated by over 4 Å. This region is pivotal in the allosteric transition between active and inactive states.

somewhat daunting to propose a specific mechanism of allosteric communication based on the comparison of inactivated and active enzyme from prokaryotic and eukaryotic sources (44% sequence identity between yeast and *E. coli* PK's). A fully validated, unambiguous model awaits the direct comparison of the T and activated (R) state enzymes from the same species as well as the structure of PK from that species complexed only with FBP. Further modeling of the mechanism of allosteric communication is, however, facilitated by our identification of the exact location of the FBP-binding site.

In order to begin modeling the mechanism of allosteric communication, the structures of the FBP-bound YPK monomer, the FBP-regulated apoenzyme monomer from *E. coli*, and the pyruvate-bound, unregulated enzyme monomer from rabbit muscle were superimposed, and the active-site structures directly compared. The overall rms deviation between Cα atoms of YPK and rabbit M_1 PK is 1.95 Å, and 3.02 Å between YPK and *E. coli* apo PK. In both cases these differences arise mainly from rotations of domains B and C relative to the A domain. (Rms deviation between the A domains of YPK and these enzymes is less than 1.17 Å for both structures). There are two significant differences between the activated and inactivated catalytic sites (Figure 8), consisting of previously noted movements of active-site residues Asp266 and Phe214 [15,26]. Phe214 may help in increasing the hydrophobicity contrast function for the metal [59], serve to pack and align the substrates correctly, and may interact directly with ADP. Asp266 directly coordinates the bound divalent cation and triggers the allosteric response in agreement with the measured thermodynamic coupling parameters for allosteric activation of YPK by metal binding [22,36].

How might FBP binding trigger the large conformational change hypothesized on the basis of these different structures? The overall nature of the conformational change consists of subunit rotations centered around distinct pivot points at the tetramer interfaces (Figure 9). In the YPK structure, the interface that is closest to the FBP-binding site contains two pairs of symmetry-related helices of the C domain packed against one another (Cα1 against Cα1′, and Cα2 against Cα2′). Salt bridges between Arg369 and Asp366′ of a neighboring subunit (as well as the reverse Asp366 and Arg369′ interaction) stabilize the interaction between helices Cα1 and Cα1′ of YPK; these helices are truncated and disordered in the *E. coli* structure and do not contribute to the tetramer interface. In contrast, helices Cα2 and Cα2′ appear to rotate and alter their packing contacts as a result of enzyme activation. In yeast the Cα2–Cα2′ interaction is created by hydrogen bonds between Glu392 and Thr376′ (and vice versa) and hydrogen bonds between the sidechain of Ser385 and the carbonyl of Ser385′ (and vice versa). These helices are separated by over 4 Å in the *E. coli*

tetramer and do not contribute to the tetramer interface. A small rotation and shear of the *E. coli* Cα2 helices inwards towards the tetramer center, forming a structure similar to activated PK, would create symmetry-related salt bridges between Arg360 and Glu364 of the *E. coli* structure. The differences between the T and R state can be accounted for in part by such a rotation. The Cα2 helices in the tetramer interface are directly adjacent to the residues forming the FBP-binding pocket within the primary sequence and 3D structure of the protein (Figure 3c). Specifically, the end of helix Cα2 occurs at Gln393 and is followed by a short five-residue β strand (Cβ1) which is then immediately followed by the protein loop that binds the 1′-phosphate of FBP.

The third part of the dimer-of-dimers interface in this region is formed by an extension of the C domain's central five-stranded β sheet across the interface, with Cβ5 and Cβ5′ forming an antiparallel interaction. When this now ten-stranded extended β sheet from *E. coli* and yeast is superimposed, it is obvious that the Cβ1 and Cβ1′ strands are slightly twisted and translated in the sheet, in order to make room for FBP binding at their C-terminal ends. This movement is propagated to the Cα2 helix and is likely to be responsible for communication of FBP binding to the tetramer interface. All of the residues within Cα1, Cα2, Cβ1, and the phosphate-binding loop are altered in humans by alternative splicing of the ninth and tenth exons in the PK M gene.

Changes at the allosteric site also include two disordered loops (residues 445–455 and residues 485–492) surrounding the FBP molecule, which become more ordered upon FBP binding. Two FBP molecules lie directly across from each other at the interface of the C domains and are ~20 Å apart. The changes in this region are likely to be responsible for the positive and negative cooperativity that is observed for FBP upon binding to the YPK–K–Mn^{2+}–PEP complex (Figure 5).

The interface between the A domains of opposite subunits is also different in the yeast and *E. coli* structures. The differences are similar to those noted in the comparison the of the bacterial and rabbit muscle enzymes and relate to the contacts made by Arg312 [15]. In the inactive *E. coli* enzyme Arg312 forms a salt bridge with Asp317′, whereas in the yeast and rabbit structure Arg312 points towards Asp147′ from the opposite B domain (although this distance is >3 Å in both the rabbit and yeast structures). In the yeast structure Asp317 now forms a salt bridge with Arg264′. These rearrangements are related to a change in the relative orientation of the opposing catalytic A domains.

Mutational analysis further supports the importance of these interfaces for enzyme regulation. In yeast, the site-directed mutation of Ser385→Pro produces a protein which requires FBP for enzyme activity [60]. This residue makes important hydrogen bonds at the Cα2–Cα2′ interface. A mutation in the rat M_1 isozyme, Ala369→Arg, causes this non-regulated muscle enzyme to exhibit sigmoidal kinetics [61]. An arginine is conserved at this position in all eukaryotic allosterically regulated isozymes, and forms part of a salt bridge between Cα1–Cα1′ in the yeast structure. Mutations in the human R isozyme expressed in red blood cells are the most common cause of hereditary nonspherocytic hemolytic anemia [62]. These mutations cluster at the active site, A domain interface and C domain [58]. In the C domain, 14 different mutations that cause this condition have been found: six are encoded in the sequence corresponding to the alternatively spliced exon of the human M gene. Two of these mutations are notable in that they impair allosteric activation of the R isozyme by FBP [63,64]. Arg405 (human R mutation Arg479→Pro) is located in the phosphate-binding loop of the FBP pocket. Ala394 (human R mutation Ala468→Val) is located in the turn between Cα2 and Cβ1, the region we propose as being important for communication between the allosteric site and the tetrameric interface.

Assuming that the *E. coli* enzyme is a representative apo structure, the change in the position of Asp266 in the quinternary complex may be a result of the metal ion mediated allosteric relay mechanism for YPK [22,36]. We propose that upon binding metal, and in the presence of substrate, Asp266 moves into the coordination sphere of the metal. This movement then triggers a change in the protein structure across either or both subunit interfaces resulting in the large domain rotations. Although these large domain motions may not significantly alter the position of key substrate or allosteric effector binding residues, they induce subtle movements of the structure in these regions and that may be all that is required to increase the binding affinity for either substrate or allosteric effector by 1–3 kcal/mol upon the binding of the metal.

Biological implications

The two main regulated steps in glycolysis are the phosphorylation of fructose-6-phosphate by phosphofructokinase (PFK) to form fructose-1,6-bisphosphate (FBP), the third step in glycolysis, and the dephosphorylation of phosphoenolpyruvate (PEP) by pyruvate kinase (PK) to form pyruvate (the final step prior to anaerobic fermentation or oxidative decarboxylation). Both of these enzymes are controlled by multiple allosteric ligands: PFK is inhibited by ATP and by citrate, and activated by AMP, while certain isozymes of PK are activated by FBP. Transient inhibition of PK activity leads to the accumulation of most glycolytic intermediates and an enhancement of gluconeogenesis.

The importance of the allosteric regulation of PK is demonstrated by a variety of studies in both mammalian and yeast systems. Studies of many tumor cell lines indicate a reproducible isozyme shift towards regulated, fetal isozymes of PK. In addition, an overall increase in levels of glycolysis has been found in these tissues. The alternatively expressed isozymes in tumor cells also commonly show increases in phosphorylation levels, another route to the regulation of the enzyme [5,7,9,10, 12]. In red blood cells, a large number of mutations in the main PK isoform have been shown to interfere with allosteric regulation. These mutations lead to an inherited form of anemia caused by an increase in the concentration of 2,3-diphosphoglycerate (a hemoglobin regulator produced by diphosphoglycerate mutase from the glycolytic intermediate 1,3-diphosphoglycerate), and result in a decrease in the affinity of hemoglobin for oxygen [65]. Finally, recent studies have demonstrated that an enzyme that phosphorylates PK in yeast is an important regulator of cell-cycle progression in that organism [66].

The studies reported here describe the allosteric FBP-binding site and the mode of PK activation by FBP. They also directly demonstrate the basis for differences in the regulatory properties of the enzyme produced by the alternative splicing of a single exon in its primary sequence. This exon contributes several residues to the FBP-binding pocket and forms the majority of the tetramer interface. This region also creates a pivot point for the subunit movements seen when comparing the activated and unactivated forms of the enzyme. The conformational differences in the active site observed between the activated, substrate-bound PK structures described here, and the structure of a low affinity, inactivated apoenzyme from *Escherichia coli* clearly demonstrate that allosteric activation is limited to small movements of a limited number of sidechains involved in binding substrate and metal ions.

Materials and methods

Purification

PK was purified from *S. cerevisiae* PYK1-500 using a modification of the previously described procedure [36]. This yeast strain contains the plasmid pPYK101 and overexpresses PK. The purification involved two chromatography steps, DEAE cellulose (Sigma) and phosphocellulose (Sigma), and NH_4SO_4 backwashes. Briefly, DEAE cellulose was equilibrated with 10 mM K_2PO_4, 5 mM EDTA, 5 mM β-mercaptoethanol (BME), pH 7.0, and the lysate, prepared by osmotic rupture using lyticase, was applied. The resin was washed with the equilibration buffer described above and the effluent solution containing the enzyme activity was then separated and adjusted to pH 6.0 using 1M HCl. A phosphocellulose slurry in 10 mM K_2PO_4, 5 mM EDTA, 5 mM BME, pH 6.0 was added to the DEAE effluent solution. After 1 h <0.6% of the total activity remained unbound in the supernatant, and this was then discarded. The phosphocellulose slurry was washed with 10 mM K_2PO_4, 25% glycerol, 5 mM EDTA, 5 mM BME, pH 6.0, and proteins were then eluted from the column with a linear gradient from 0 to 0.6 M KCl in 10 mM K_2PO_4, 25% glycerol, 5 mM EDTA, 5 mM BME, pH 6.0. Fractions with greater than 190 units/ml PK activity (eluted between 0.35 to 0.45 M KCl) were pooled for further purification. The pooled fractions were concentrated to greater than 10 mg/ml. The concentrated protein was then dialyzed overnight against 10 mM K_2PO_4, 25% glycerol, 5 mM EDTA, 5 mM BME, pH 6.2 saturated with NH_4SO_4. The precipitated protein was centrifuged and the supernatant removed. The protein pellet was then washed with 10 mM K_2PO_4, 25% glycerol, 5 mM EDTA, 5 mM BME, pH 6.2 saturated with 56, 54, 48 and 44% NH_4SO_4. The washes were performed in descending succession. Supernatants with PK activity greater than 200 units/mg were combined and concentrated to greater then 10 mg/ml. The purified enzyme, at a concentration of 10–15 mg/ml, was stored at 4°C as a suspension in 46% saturated NH_4SO_4, 200 mM KCl, 10 mM phosphate, 20% glycerol, 5 mM BME, pH 6.2. The enzyme was desalted for further experiments by centrifugation and resuspension of the pellet in 20% glycerol, 200 mM KCl, 10 mM phosphate pH 6.2, and then passed over a Pharmacia dextran 200 sizing column equilibrated with the same buffer. The enzyme was found to be relatively unstable when stored in the absence of NH_4SO_4, therefore only volumes of enzyme required for immediate use were resuspended.

Steady-state kinetic studies

YPK activity was measured by a continuous assay coupled to lactate dehydrogenase (LDH). The change in absorbance at 340 nm due to oxidation of NADH was measured using either a Hewlet-Packard 7475A diode array or a Gilford 240 or 250 UV/VIS thermostated spectrophotometer. Kinetic assays for specific activity determinations contained YPK (0.5 to 0.7 μg), MES (100 mM), glycerol (5%), KCl (200 mM), $MgCl_2$ (15 mM), ADP (5 mM), PEP (5 mM), FBP (1 mM), NADH (175 μM), and LDH (20 μg). PG inhibition studies were performed under the same assay conditions listed above except Mn^{2+} at 10 mM was substituted for Mg^{2+} and the FBP concentration was fixed at 10 mM. The substrate PEP was varied from 5 to 200 mM at fixed, variable PG concentrations. PG activation studies were performed by varying PG concentrations at fixed, variable PEP concentrations in the absence of FBP. Steady-state kinetic rates were determined by measuring the slope of the tangent to the reaction progress curve. All initial velocity data was first fit to both the Michaelis–Menten and the Hill equations for the determination of the apparent Michaelis constants (K_M), Hill coefficients (n_H), and maximal velocity (V_{max}) using the program Table Curve 2D (Jandel Scientific). PG inhibition data was then fit to models for competitive, non-competitive and uncompetitive inhibition using the program Table Curve 3D (Jandel Scientific).

Crystallization

Crystallization experiments were carried out using the method of vapor diffusion in hanging drops. Protein concentrations ranged from 4–12 mg/ml in the experiments. Two separate complexes of YPK were co-crystallized. The first was a quaternary complex of YPK complexed with PG (10 mM) and Mn^{2+} (10 mM) in 200 mM KCl. The second complex was a quinternary complex similar to the first except that 10 mM FBP was added. The crystallization solution in the reservoir for the quaternary complex co-crystallization had a volume of 300 μl and was composed of 28–33% (w/v) PEG 8000, 200 mM sodium acetate, 100 mM sodium cacodylate pH 6.5. 2 μl of the protein solution and 2 ml of the reservoir solution were mixed and then equilibrated against the reservoir at 4°C for 1–16 weeks before crystals appeared. The dimensions of the crystals used were 0.4 mm × 0.2 mm × 0.2. The quinternary complex co-crystallization was similar to that of the quaternary complex, except that the best crystals were grown using a reservoir with a volume of 600 μl, composed of 34–36% (w/v) PEG 8000, 50 mM sodium acetate, 100 mM sodium cacodylate pH 6.5. The crystals were allowed to grow at 4°C but for a longer period of time, 2–6 months, before X-ray quality crystals were obtained. The quaternary complex crystals grew in space group C2 with cell dimensions a = 108.3, b = 106.4, c = 105.5 Å, β = 110.8°C, with two monomers of PK forming the asymmetric unit. The quinternary complex crystals also grew in space group C2 with cell dimensions a = 110.4, b = 104.0, c = 112.2 Å, β = 112.3°C, and two monomers of PK in an asymmetric unit.

Data collection

Diffraction data for the quinternary complex were collected on an RAXIS II area detector. The X-ray source was CuK_α radiation from a Rigaku RU-200 rotating anode operated at 50 kV and 100 mA, with a graphite monochromator. The crystal form of the quinternary complex was mounted in a capillary tube and data were collected at 10°C. Diffraction data for the quaternary complex was collected at the Brookhaven National Synchrotron Light Source on beamline X12-C using a MAR RESEARCH area detector. The crystal of the quaternary complex was flash-cooled at −175°C after equilibration of the crystal with a cryo-solvent containing 20% glycerol, 40 % PEG 8000, 200 mM KCl, and 10 mM phosphate buffer at pH 6.5. All data was processed using DENZO and SCALEPACK [67] (results shown in Table 1).

Molecular replacement

The structure of YPK was solved by molecular replacement (MR) with the AMORE software package [68]. The coordinates of PK from rabbit muscle were used as the search model. All the sidechains in the model that were known from sequence alignment to be different from yeast enzyme were converted to alanine using the modeling package QUANTA. For the rotation function only Patterson densities inside a spherical shell of inner and outer radii of 3 Å and 35 Å were used in Patterson map superpositions.

For the quinternary enzyme complex, the structure was solved using an enzyme monomer as the search model in MR (the asymmetric unit is a pair of subunits). Within the highest rotation peaks the first and third are related by 180°C. These two solutions were assumed to represent orientations of the two molecules in the asymmetric unit. The locations of the two molecules were then determined by the corresponding translation function calculation. The highest (and next highest) correlation coefficients calculated for peaks in the translation maps for the two orientations are 24.1 and 22.3 (18.6), respectively. These highest correlation coefficients also correspond to the lowest R factors. For the relative y separation between the two molecules, the translation function for the second orientation was calculated with the first solution fixed, and yielded a single large peak with correlation coefficient of 35.8. Rigid-body refinement of the orientation and position of the two molecules using data between 10.0 Å and 3.0 Å resulted in a crystallographic R factor of 47.7%

For the quaternary enzyme complex, the structure was solved using a monomer of the refined quinternary complex as a the search model in MR. The highest two peaks in the rotation search have correlation coefficients of 23.1 and 20.5 and are related by a rotation of 180°C. The next highest peak is considerably weaker at 8.8. The translation search solutions for these orientations yielded peaks with correlation coefficients of 37.9 and 32.4. By fixing on monomer and repeating the translation search for the other monomer and vice versa, further refinement of these positions were obtained with correlation coefficients of 60.1 and 60.7. Rigid-body refinement of the orientation and position of the two molecules using data between 10.0 Å and 3.5 Å resulted in a crystallographic R factor of 36.1%.

Table 1

Data collection and refinement statistics.

	Quinternary complex (+FBP)	Quaternary complex (–FBP)
Space group	C2	C2
Cell parameters (Å) (a, b, c)	110.4, 104.0, 112.2	108.3, 106.4, 105.5
β (°)	112.3	110.8
Crystalline forms	Monoclinic	Monoclinic
No. molecules/asymmetric unit	2	2
No. reflections	66 108	94 232
No. unique reflections	19 294	19 331
R_{sym} (%)	6.5	10.8
Refinement		
Resolution range (Å)	100–3.0	100–3.0
Unique reflections ($F > 2\sigma$)	17 327	18 430
Completeness (%)	91	85
R factor (no σ cut-off) (%)	21.8 (24.8)	22.7 (24.8)
R free (no σ cut-off) (%)	32.3 (34.9)	34.1 (34.3)
No. of protein atoms in final model (no solvent molecules included)	7524	7476
Ramachandran plot		
core (%)	80.5	76.3
allowed (%)	16.6	19.2
generous (%)	2.1	3.5
disallowed (%)	0.8	0.9
Rmsd		
bonds (Å)	0.009	0.013
angles (°)	1.868	1.736
dihedrals (°)	27.69	24.480
impropers (°)	0.930	1.571
Average B factor (Å^2)	25	14
B factor (Å^2)/occupancy (%)		
FBP	28/87	–
Phosphoglycolate	35/87	16/93
Mn^{2+}	18/100	10/100
K^+	29/84	15/100

Modeling and refinement

Prior to any refinement 10% of the data was set aside for cross validation with R_{free}. Refinement of the quinternary complex was performed with X-PLOR [69]. Following an initial positional refinement PG, Mn^{2+}, and K^+ were built into the active site using a $F_o–F_c$ map contoured at 1.7σ. Iterative rounds of simulated annealing, torsional and positional refinement failed to result in a significant drop in R_{free} until noncrystallographic symmetry (NCS) restraints and a bulk-solvent correction were employed. NCS restraints were applied by grouping the A and C domains separately from the B domains. This was to account for a small shift in the positions between the two B domains relative to the rest of the protein. The rms deviation between NCS related Cα atoms was 0.17 Å for the A and C domains, and 0.13 Å for the B domains. $2F_o–F_c$ and $F_o–F_c$ maps were used to manually rebuild sidechains and adjust the model. After a group B refinement the R factor was 23.4% and R_{free} was 34.8%. At this point FBP was built into the allosteric site using a $F_o–F_c$ map contoured at 3.5σ. The map presented strong density for the two phosphate groups of FBP, and the bridging ribose sugar ring. Occupancy refinement for all modeled ligands was performed to confirm their placement in the electron density. The final model for the asymmetric unit of the activated quinternary complex contains two FBP molecules, two PG molecules, two Mn^{2+} ions, two K^+ ions, and two protein subunits consisting of 500 residues each (except for the loop of residues 11–16 and turn of residues 160–161 in both subunits and the turn of residues 99–101 in the second subunit).

Refinement of the quaternary complex was straight forward (Table 1). NCS restraints were employed in XPLOR with rounds of simulated annealing, torsional and positional refinement. $2F_o–F_c$ and $F_o–F_c$ maps were used to check and adjust the model. The R factor, R_{free} and Ramachandran plots were used to gauge the progression of the refinement. Strong difference density (>4σ) was present in the active site for the two cations and PG, and these were built into the model. There was no difference density in the FBP-binding site and the loop of residues 446–452 was not present in the $2F_o–F_c$ map. Also, no density was present for the loop of residues 485–493. These residues were removed from the model in both subunits.

There are four to five Ramachandran outliers per subunit (500 residues/subunit total). One of these is present in a turn of the A domain (Lys233) and is well defined in the density. The remaining outliers are in less well-defined loops, primarily in the B domain. Overall the density of the B domain is of poorer quality, as illustrated by higher B factors and a large proportion of generously allowed Ramachandran angles in this region. NCS restraints in this region were used with caution but still resulted in improvement of the structure as monitored by R_{free}.

Accession numbers

Coordinates for the structures of the quaternary and quinternary complexes have been deposited in the PDB with ID codes 1A3X and 1A3W, respectively.

Acknowledgements

This work was supported by grants from the NIH to BLS and TN and by a fellowship from the NSF to MSJ. We also acknowledge crystal growth experiments by Sheryl Oelke, help with YPK purification by Patrick Loria, and the support of Brookhaven beam line X-12C staff scientists during data collection.

References

1. Noguchi, T., Yamada, K., Inoue, H., Matsuda, T. & Tanaka, T. (1987). The L- and R-type isozymes of rat pyruvate kinase are produced from a single gene by use of different promotors. *J. Biol. Chem.* **143**, 431-438.
2. Noguchi, T., Inoue, H. & Tanaka, T. (1986). The M1 and M2 -type isozymes of rat pyruvate kinase are produced from the same gene by alternative RNA splicing. *J. Biol. Chem.* **261**, 13807-13812.
3. El-Maghrabi, M.R., Claus, T.H., McGrane, M.M. & Pilkis, S.J. (1982). Influence of phosphorylation on the interaction of effectors with rat liver pyruvate kinase. *J. Biol. Chem.* **257**, 233-237.
4. Staal, E.J. & Rijksen, G. (1985). Regulation of pyruvate kinase in normal and pathological conditions. In *Regulation of Carbohydrate Metabolism* (Beitner, R. eds), pp.143-159, CRC Press, Boca Raton, FL.
5. van Veelen, W.M., Verbiest, H., Vlug, A.M.C., Rijksen, G. & Staal, E.J. (1978). Isozymes of pyruvate kinase from human brain, meningiomas, and malignant gliomas. *Cancer Res.* **38**, 4681-4687.
6. van Veelen, W.M., *et al.*, & Staal, E.J. (1979). Lα-Alanine inhibition of pyruvate kinase from tumors of the human central nervous system. *Cancer Res.* **39**, 4263-4269.
7. van Veelen, W.M. & Staal, E.J. (1985). Pyruvate kinase and human brain tumors. In *Markers of Human Neuroectodermal Tumors* (Staal, E.J. & van Veelen, W.M. eds), pp.63-83, CRC Press, Boca Raton, FL.
8. Ibsen, K., Orlando, R.A., Garratt, K.N., Hernandez, A.M., Giorlando, S. & Nungaray, G. (1982). Expression of multimolecular forms of pyruvate kinase in normal, benign, and malignant human breast tissue. *Cancer Res.* **42**, 888-892.
9. Balinsky, D., Platz, C.E. & Lewis, J.W. (1983). Isozyme patterns of normal, benign, and malignant human breast tissues. *Cancer Res.* **43**, 5895-5901.
10. Hennipman, A., *et al.*, & Staal, G.E. (1987). Glycolytic enzymes in breast cancer, benign breast disease and normal breast tissue. *Tumour Biol.* **8**, 251-263.
11. Rijksen, G., van der Heijden, M.C., Oskam, R. & Staal, G.E.J. (1988). Subunit-specific phosphorylation of pyruvate kinase in medullary thyroid carcinomas of the rat. *FEBS Lett.* **233**, 69-73.
12. Weernink, A., Rijksen, G., van der Heijden, M.C.M. & Staal, G.E.J. (1990). Phosphorylation of pyruvate kinase type K in human gliomas by a cyclic adenosine 5′-monophosphate-independent protein kinase. *Cancer Res.* **50**, 4604-4610.
13. Stuart, D.I., Levine, M., Muirhead, H. & Stammers, D.K. (1979). Crystal structure of cat pyruvate kinase at a resolution of 2.6 Å. *J. Mol. Biol.* **134**, 109-142.
14. Speranza, M.L., Valentini, G., Iadarola, P., Stoppini, M., Malcovati, M. & Ferri, G. (1989). Primary structure of three peptides at the catalytic and allosteric sites of the fructose-1,6-bisphosphate-activated pyruvate kinase from *Escherichia coli*. *Biol. Chem. Hoppe Seyler* **370**, 211-216.
15. Mattevi, A., Valentini, G., Rizzi, M., Speranza, M.L., Bolognesi, M. & Coda, A. (1995). Crystal structure of *Escherichia coli* pyruvate kinase type I: molecular basis of the allosteric transition. *Structure* **3**, 729-741.
16. Larsen, T.M., Laughlin, T., Holden, H.M., Raymont, I. & Reed, G.H. (1994). Structure of rabbit muscle pyruvate kinase complexed with Mn^{2+}, K^+, and pyruvate. *Biochemistry* **33**, 6301-6309.
17. Allen, S.C. & Muirhead, H. (1996). Refined three-dimensional structure of cat-muscle (M1) pyruvate kinase at a resolution of 2.6 Å. *Acta. Cryst. D* **52**, 499-504.
18. Mesecar, A. (1994). *Kinetic Responses and Conformational Changes Required for Yeast Pyruvate Kinase Activation and Catalysis*. PhD Thesis, University of Notre Dame, IN.
19. Pierce, J., Serianni, A.S. & Barker, R. (1985). Anomerization of furanose sugars and sugar phosphates. *J. Am. Chem. Soc.* **107**, 2448-2456.
20. Fishbein, R., Benkovic, P.A. & Benkovic, S.J. (1975). The anomeric specificity of yeast pyruvate kinase toward the activation by D-fructose-1,6-bisphosphate. *Biochemistry* **14**, 4060-4063.
21. Wurster, B. & Hess, B. (1976). Tautomeric and anomeric specificity of allosteric activation of yeast pyruvate kinase by D-fructose-1,6-bisphosphate and its relevance in D-glucose catabolism. *FEBS Lett.* **63**, 17-21.
22. Mesecar, A.D. & Nowak, T. (1997). Metal-ion-mediated allosteric triggering of yeast pyruvate kinase. 1. A multidimensional thermodynamic linked-function analysis. *Biochemistry* **36**, 6803-6813.
23. Valentini, G., Speranza, M.L., Iadarola, P., Ferri, G. & Malcovati, M. (1988). Reactivity of the fructose-1,6-bisphosphate-activated pyruvate kinase from *Escherichia coli* with pyridoxal 5′-phosphate. *Biol. Chem.* **369**, 1219-1226.
24. Leblond, D. & Robinson, J. (1976). Secondary kinase reactions catalyzed by yeast pyruvate kinase. *Biochim. Biophys. Acta* **438**, 108-118.
25. Koshland, D., Nemethy, G. & Filmer, D. (1966). Comparison of experimental binding data and theoretical models in proteins containing subunits. *Biochemistry* **5**, 365-385.

26. Larsen, T.M., Benning, M.M., Wesenberg, G.E., Rayment, I. & Reed, G.H. (1997). Ligand-induced domain movement in pyruvate kinase: structure of the enzyme from rabbit muscle with Mg^{2+}, K^+, and L-phospholactate at 2.7 Å resolution. *Arch. Biochem. Biophys.* **345**, 199-206.
27. Westheimer, F.H. (1987). Why nature chose phosphates. *Science* **235**, 1173-1178.
28. Orr, G.A., Simon, J., Jones, S.R., Chin, G.J. & Knowles, J.R. (1978). Adenosine-5′-O-([γ-18O]- γ-thio)triphosphate chiral at the γ-phosphorous: stereochemical consequences of reactions catalyzed by pyruvate kinase, glycerol kinase, and hexokinase. *Proc. Natl. Acad. Sci. USA* **75**, 2230-2233.
29. Hasset, A., Blattler, W. & Knowles, J.R. (1982). Pyruvate kinase: is the mechanism of phospho transfer associative or dissociative? *Biochemistry* **21**, 6335-6340.
30. Dann, L.G. & Britton, H.G. (1978). Kinetics and mechanism of action of muscle pyruvate kinase. *Biochem. J.* **169**, 39-54.
31. Seeholzer, S.H., Jaworoski, A. & Rose, I.A. (1991). Enolpyruvate: chemical determination as a pyruvate kinase intermediate. *Biochemistry* **30**, 727-732.
32. Nowak, T. & Suelter, C. (1981). Pyruvate kinase: activation by and catalytic role of the monovalent and divalent cations. *Mol. Cell. Biochem.* **35**, 65-75.
33. Baek, Y.H. & Nowak, T. (1982). Kinetic evidence for a dual cation role for muscle pyruvate kinase. *Arch. Biochem. Biophys.* **217**, 491-497.
34. Mildvan, A.S. & Cohn, M. (1966). Kinetic and magnetic resonance studies of the pyruvate kinase reaction. II. Complexes of enzyme, metal, and substrates. *J. Biol. Chem.* **241**, 1178-1193.
35. Nowak, T. & Lee, M.J. (1977). Reciprocal cooperative effects of multiple ligand binding to pyruvate kinase. *Biochemistry* **16**, 1343-1350.
36. Mesecar, A.D. & Nowak, T. (1997). Metal-ion-mediated allosteric triggering of yeast pyruvate kinase. 2. A multidimensional thermodynamic linked-function analysis. *Biochemistry* **36**, 6803-6813.
37. Glusker, J. (1991). Structural aspects of metal liganding to functional groups in proteins. *Adv. Protein Chem.* **42**, 1-76.
38. Loria, J.P. (1997). *Active Site Structure and Conformational Changes in Yeast Pyruvate Kinase*. PhD Thesis, University of Notre Dame, IN.
39. Waygood, E.B., Rayman, M.K. & Sanwal, B.D. (1975). The control of pyruvate kinases of *Escherichia coli*. II. Effectors and regulatory properties of the enzyme activated by ribose 5-phosphate. *Can. J. Biochem.* **53**, 444-452.
40. Jetten, M.S., Gubler, M.E., Lee, S.H. & Sinskey, A.J. (1994). Structural and functional analysis of pyruvate kinase from *Corynebacterium glutamicum*. *Appl. Environ. Microbiol.* **60**, 2501-2507.
41. Gupta, R.K., Oesterling, R.M. & Mildvan, A.S. (1976). Dual divalent cation requirements of activation of pyruvate kinase: essential roles of both enzyme and nucleotide-bound metal ions. *Biochemistry* **15**, 2881-2887.
42. Cottam, G.L., Mildvan, A.S., Hunsley, J.R. & Suelter, C.H. (1972). Proton relaxation and kinetic studies of ternary complexes of an allosteric pyruvate kinase from yeast. *J. Biol. Chem.* **247**, 3802-3809.
43. Mechitsuka, S., Smith, G.M. & Mildvan, A.S. (1981). Proton NMR studies of histidine residues and of bound ATP on rabbit muscle pyruvate kinase. *J. Biol. Chem.* **256**, 4460-4465.
44. Gupta, R.K. (1977). A novel nuclear relaxation approach for estimating distance between enzyme- and nucleotide-bound metal ions at the catalytic site of pyruvate kinase. *J. Biol. Chem.* **252**, 5183-5185.
45. Gupta, R.K. & Benovic, J.L. (1978). Magnetic resonance and kinetic studies of the spatial arrangement of phosphoenolpyruvate and chromium (III)-adenosine diphosphate at the catalytic site of pyruvate kinase. *J. Biol. Chem.* **253**, 8878-8886.
46. Van Divender, J.M. & Grisham, C.M. (1985). ^7Li, ^{31}P, and ^1H NMR studies of interactions between ATP, monovalent cations, and divalent cation sites on rabbit muscle pyruvate kinase. *J. Biol. Chem.* **260**, 14060-14069.
47. Imarai, M., Hinrichsen, P., Bazaes, S., Wilkens, M. & Eyzaguirre, J. (1988). Yeast pyruvate kinase: essential lysine residues in the active site. *Int. J. Biochem.* **20**, 1001-1008.
48. Valentini, G., Iadarola, P., Ferri, G. & Speranza, M.L. (1995). Affinity labeling of the catalytic and allosteric ATP binding sites on pyruvate kinase type 1 from *Escherichia coli*. *Biol. Chem. Hoppe Seyler* **376**, 231-235.
49. Bezares, G., *et al*., & Bazaes, S. (1987). Isolation and sequence determination of an active site peptide of rabbit muscle pyruvate kinase. *Arch. Biochem. Biophys.* **253**, 133-137.
50. Waygood, E.B. & Sanwal, B.D. (1974). The control of pyruvate kinases of *Escherichia coli*.1. Physiochemical and regulatory properties of the enzyme activated by fructose 1,6-diphosphate. *J. Biol. Chem.* **249**, 265-274.
51. Carminatti, H., Jimenez de Asua, L., Recondo, E., Passeron, S. & Rozengurt, E. (1968). Some kinetic properties of liver pyruvate kinase (Type L). *J. Biol. Chem.* **243**, 3051-3056.
52. Plowman, K.M. & Krall, A.R. (1965). A kinetic study of nucleotide interactions with pyruvate kinase. *Biochemistry* **4**, 2809-2814.
53. Rosevear, P.R., Fox, T.L. & Mildvan, A.S. (1987). Nuclear Overhauser effect studies of the conformations of MgATP bound to the active and secondary sites of muscle pyruvate kinase. *Biochemistry* **26**, 3487-3493.
54. Ford, S.R. & Robinson, J.L. (1976). The proton transfer reactions catalyzed by yeast pyruvate kinase. *Biochim. Biophys. Acta* **438**, 119-130.
55. Mesecar, A.D., Stoddard, B.L. & Koshland, D.E. (1997). Orbital steering in the catalytic power of enzymes: small structural changes with large catalytic consequences. *Science* **16**, 202-206.
56. Kinderlerer, J., Ainsworth, S., Morris, C.N. & Rhodes, N. (1986). The regulatory properties of yeast pyruvate kinase. Effect of pH. *Biochem. J.* **243**, 699-703.
57. Rhodes, N., Morris, C.N., Ainsworth, S. & Kinderlerer, J. (1986). The regulatory properties of yeast pyruvate kinase. Effects of NH^{4+} and K^+ concentrations. *Biochem. J.* **234**, 705-715.
58. Mattevi, A., Bolognesi, M. & Valentini, G. (1996). The allosteric regulation of pyruvate kinase. *FEBS Lett.* **389**, 15-19.
59. Yamashita, M.M., Wesson, L., Eisenman, G. & Eisenberg, D. (1990). Where metal ions bind in proteins. *Proc. Natl. Acad. Sci. USA* **87**, 5648-5652.
60. Collins, R.A., McNally, T., Fothergill-Gilmore, L.A. & Muirhead, H. (1995). A subunit interface mutant of yeast pyruvate kinase requires the allosteric activator fructose 1,6-bisphosphate for activity. *Biochem. J.* **310**, 117-123.
61. Ikeda, Y., Tanka, T. & Noguchi, T. (1997). Conversion of non-allosteric pyruvate kinase isozyme into an allosteric enzyme by a single amino acid substitution. *J. Biol. Chem.* **272**, 20495-20501.
62. Beutler, E. & Baronciani, L. (1996). Mutations in pyruvate kinase. *Human Mutation* **7**, 1-6.
63. Kanno, H., Ballas, S.K., Miwa, S., Fujii, H. & Bowman, H.S. (1994). Molecular abnormality of erythrocyte pyruvate kinase deficiency in the Amish. *Blood* **83**, 2311-2316.
64. Kanno, H., *et al*., & Miwa, S. (1994). Hereditary hemolytic anemia caused by diverse point mutations of pyruvate kinase gene found in Japan and Hong Kong. *Blood* **84**, 3505-3509.
65. Miwa, S., Kanno, H. & Fuji, H. (1993). Pyruvate kinase deficiency: historical perspective and recent progress of molecular genetics. *Am. J. Hematol.* **42**, 31-35.
66. Brazill, D.T., Thorner, J. & Martin, G.S. (1997). Mck1, a member of the glycogen synthase kinase 3 family of protein kinases, is a negative regulator of pyruvate kinase in the yeast *Saccharomyces cerevisiae*. *J. Bacteriol.* **179**, 4415-4418.
67. Otwinowski, Z. (1993). DENZO. In *Data Collection and Processing.* (Sawyer, L., Isaacs, N. & Bailey, S. eds.), pp.56-62, SERC Daresbury Laboratory, Warrington, UK.
68. Navaza, J. (1994). AMORE: an automated procedure for molecular replacement. *Acta Cryst. A* **50**, 157-163.
69. Brünger, A.T. (1987). Crystallographic R-factor refinement by molecular dynamics. *Science* **235**, 458-460.